THE DYNAMIC STABILITY UNDER IMPULSIVE LOADING OF SHALLOW ARCHES WITH ELASTIC END RESTRAINTS

Thesis by

Terry Joseph Delph

In Partial Fulfillment of the Requirements

For the Degree of

Aeronautical Engineer

California Institute of Technology

Pasadena, California

1969

ACKNOWLEDGMENT

The author wishes to express his appreciation to Dr. C. D. Babcock, Jr. for his valuable guidance and advice during the course of this work. Thanks are also due to Dr. M. C. Cheung, and to Mr. Clarence Hemphill of the Electronics Laboratory, for their patient help. Miss Helen Burrus and Mrs. Betty Wood were responsible for the typing and the figures respectively, and their assistance is gratefully recognized.

This study was supported by the Air Force Office of Scientific Research, Office of Aerospace Research, United States Air Force under Grant Number AFOSR 68-1424.

ABSTRACT

A theoretical and experimental study of the buckling under impulsive load of an arch with rotational end restraints was carried out.

Impulsive loading was realized experimentally by use of the spray deposited explosive silver nitrate-silver acetylide. The experimental buckling loads were compared to those obtained by a theoretical analysis. It was found that the theoretical analysis yields a quite conservative lower bound on the magnitude of load necessary for buckling. Both uniform and nonuniform loadings were considered.

It was found that there exists a critical value of rotational spring constant above which dynamic buckling may not occur in the rigorous mathematical sense. An expression for this critical value was found.

TABLE OF CONTENTS

NOMENCLATURE

A	Arch cross sectional area
B	Magnitude of distributed load (lbs/in)
C	Nondimensional axial spring constant
E	Young's modulus
H	Arch end thrust
H_o	Initial arch end thrust
I	Impulse (slug-in/sec), moment of inertia
K	Rotational spring constant (in-lbs/rad)
K'	Nondimensional rotational spring constant
L	Arch length
q	Distributed arch loading (lbs/in)
r	Nondimensional initial arch rise
s	Nondimensional initial end thrust
$\bar{U}$	Dimensional strain energy
U	Nondimensional strain energy
$\bar{V}$	Dimensional energy
V	Shear force, nondimensional energy
W_e	Explosive weight (gm)
w	Arch displacement
w_o	Initial arch displacement
x	Axial arch coordinate
y	Nondimensional arch displacement
y_o	Nondimensional initial arch displacement

NOMENCLATURE (Cont'd)

α	Axial spring constant
β	Nondimensional arch end thrust
δ	Arch end deflection
ξ	Nondimensional axial arch coordinate
ρ	Mass density

LIST OF FIGURES

I. INTRODUCTION

The static and dynamic behavior of shallow arches is of much interest to the engineer, as shallow arches represent one of the simplest types of nonlinear structures which exhibit the dynamic buckling phenomenon, a feature which is common to more complex shell structures. The complete, time-dependent equation of motion for the shallow arch is given by a nonlinear partial differential equation to which an exact solution has not yet been found. If the time-dependent terms are ignored, the static equation of equilibrium results, which may be solved exactly for various types of loadings and boundary conditions (Refs. 1 and 2). However, if one wishes to treat the dynamic loading case, one must resort to energy methods, or numerical or analogue techniques for solving the complete equation of motion.

In particular, the dynamic buckling (or dynamic snap through) phenomenon has attracted attention. Dynamic buckling may best be defined as a large increase in displacement resulting from a very small increase in the magnitude of an applied, time-dependent, load. The load at which this increase in displacement occurs is known as the dynamic buckling load. This behavior has been analyzed by Hsu (Ref. 3) using an energy argument. He showed that a sufficient condition for the possibility of dynamic buckling to exist is that the system under consideration possess at least one stable equilibrium position other than the original unloaded position.

The dynamic buckling of a simply supported arch was first investigated by Hoff and Bruce (Ref. 4). Arches with clamped ends

were considered by Humphreys (Ref. 5) and Cheung (Ref. 6), among others. It may be noted that both the simply supported and clamped boundary conditions represent the limiting cases of an arch whose ends are elastically restrained in rotation. If K is the rotational spring constant, then $K = 0$ gives the simply supported boundary conditions, and $K \rightarrow \infty$ gives the clamped conditions. It was thus thought worthwhile to investigate the dynamic buckling behavior of an arch with elastically restrained ends. This thesis presents the results of that investigation.

First, a series of experiments were conducted on arches subjected to uniformly distributed impulsive loadings with the afore mentioned boundary conditions. The results are compared to the critical loads predicted by Hsu's criteria.

Secondly, some qualitative features of the potential energy function of the arch are discussed. It has been shown that dynamic buckling of an impulsively loaded clamped arch in the sense of Hsu is impossible (Ref. 7). However, dynamic buckling is possible for the simply supported arch. This suggests that there exists some value of rotational spring constant above which dynamic buckling may not occur. This is shown by a theoretical argument to actually be the case, and an expression for this critical value is given.

II. DESCRIPTION OF EXPERIMENT

A. Description of Explosive

Impulsive loading was achieved experimentally by use of the explosive silver acetylide-silver nitrate ($Ag_2C_2 \cdot AgNO_3$). This compound yields the low impulse levels necessary for an experiment of this type and is also relatively safe to handle.

The method of preparation of the explosive is discussed in reference 8. The explosive is best spray deposited, and the method of spraying is described in references 8 and 9. In this case, the spray was deposited on 0.002 in. thick strips of Mylar of the desired length. After drying, the strips could be conveniently laid on the surface to be loaded.

Silver-acetylide-silver nitrate is light sensitive, and detonation was achieved by means of a nonexpendable Xenon flash tube with a 10 in. parabolic reflector. By examination of the Mylar strips after firing, it was found that detonation occurred nearly simultaneously at several points directly beneath the flash tube. Ignition then proceeded outward from these points. Cheung (Ref. 6) has shown that the speed of propagation of the explosion is such that the resulting impulse may be considered as essentially uniform, even though uniform ignition over the explosive surface is not realized. Reference 6 also gives a more complete description of the flash tube apparatus.

In order to verify previously obtained values of impulse per unit weight of explosive, a series of tests were performed on a ballistic pendulum. The explosive for these tests was sprayed onto

1" x 4" strips of 0.002 in. Mylar in order to simulate as nearly as possible the explosive strip geometry used in the actual arch tests. The value of impulse per unit weight of explosive obtained from these tests agreed very well with that reported by Cheung (Ref. 6). This value is $I/W_e = 1.79$ slug-in/sec-gm.

It should be noted that Cheung sprayed his explosive onto a bare metal surface. Apparently, then, the Mylar surface has only an insignificant effect on the magnitude of the impulse unit weight obtainable from the explosive. However, it was observed that for values of W_e/A less than about 0.025 gm/in^2, the explosive would propagate only a short distance from the initial points of ignition, leaving the area at the ends of the strip unignited. It is hypothesized that this is a Mylar effect, as Cheung obtained complete ignition with values of W_e/A less than 0.025 gm/in^2.

A drawback to the technique of using a spray-deposited explosive should be mentioned. Although it is possible to obtain fairly uniform sprays and thus uniform loadings, it is difficult to deposit exactly a given weight of explosive. Thus one must usually spray a number of strips to obtain one with a weight close to the desired weight.

B. Apparatus

1. Arch. The arch used in the impulsive loading experiments was formed from a flat piece of spring steel 15 in. long, 1 in. wide, and 1/32 in. thick. The arch shape was obtained by buckling the strip as an Euler column, until the desired central rise was obtained. From the theory of column buckling, it is known that the resulting shape is a half-sine wave.

This is a simple means of obtaining a shallow sinusoidal arch, and avoids the necessity of rolling the strip to form the desired shape. However, an initial end thrust, approximately equal to the first Euler buckling load for the strip, is introduced into the structure. This must accordingly be taken into account in the theoretical analysis.

2. Rotational spring and arch frame. The rotational springs were constructed by attaching torsion rods to either end of the arch in such a way that rotation of the arch ends resulted in twisting of the rods. This was accomplished by securing both ends of the rod in drill chucks so that no rotation of the rod ends was possible. Two small plates were then screwed down over the center of the rod, and one end of the arch inserted between the two plates, so that the arch end rested against the rod. Two set screws in the top of one of the plates were then tightened to hold the arch in place. The center of each torsion rod was knurled, so as to reduce the possibility of slippage between the rod and the clamped plates. This arrangement is depicted in Figure 1.

To avoid lateral bending of the torsion rods due to arch end thrust, the rods were supported by passing them through Torrington 4NBC612ZP needle bearings placed immediately to either side of the clamped plates. The bearings were pressed into metal blocks which were then bolted to the arch frame, a heavy steel structure. The bearings also served to restrain the arch ends from motion. An overall view of the arch frame, with torsion rods and arch in place, is given in Figure 2a, b.

3. Spring stiffnesses. The torsion rods were made from lengths of steel rod. By varying the length and diameter of the rod, a fairly wide range of rotational spring constants could be obtained. It should be noted here that the drill chucks could be moved along the length of the crossarms, allowing the use of rods of different lengths.

After manufacturing the rods, their rotational spring constants were measured experimentally by placing the rods in position in the arch frame. They were then subjected to a known moment applied through the clamping plates and the resulting angle of twist measured. Rods having four different rotational spring constants were used in the impulsive loading experiments. These had values of $K = 85.0$, 75.0, 48.8, and 22.5 in-lbs/rad.

The torsional stiffnesses of the rods were also calculated using the standard torsional theory for circular bars. For the stiffest spring, this gave a value of stiffness 15 $^{o}/o$ above that observed experimentally. The agreement between theory and experiment became better with decreasing stiffness. It is felt that this discrepancy is due to some twisting of the rod within the clamped plates, the rods not being held completely clamped. However the experimental values of torsional stiffness were quite repeatable, so this occasioned no difficulty.

It was found that the arch frame possessed a nonnegligible amount of flexibility in the axial, or horizontal direction. The stiffness of the frame in the axial direction was accordingly measured experimentally by applying a known force over the range of expected arch end thrusts and measuring the deflection. In this manner, it

was determined that the frame had an effective axial spring constant of approximately 16,600 lbs/in. This was then included in the theoretical analysis by adding an axial spring at one end of the arch.

4. Measurement of arch deflection. A measurement of the arch deflection under loading was obtained by soldering a long needle to the underside of the arch at its center. When the arch deflected, the needle pierced a series of tissue strips. An examination of the tissues after the experiment was over then gave an indication of the total deflection of the center of the arch. Since the tissues were spaced 0.2 in. apart, only an approximate measure could be obtained. However, this is not felt to be a serious drawback. A photograph of the small frame used to hold the tissue strips is given in Figure 3.

III. THEORETICAL ANALYSIS

A. Equations of Motion

The arch geometry to be considered is shown in Figure 4a. It is assumed that due to the shallowness of the arch, the axial load H may be considered constant throughout the arch. Under this assumption, the equation of motion may be derived by considering the equilibrium of a differential element of the arch, shown in Figure 4b.

Summing forces in the vertical direction

$$\frac{\partial V}{\partial x} + q + \rho A \frac{\partial^2 w}{\partial t^2} = 0$$

and taking moments about point A,

$$\frac{\partial M}{\partial x} - V + H \frac{\partial w}{\partial x} = 0$$

Combining these equations

$$\frac{\partial^2 M}{\partial x^2} + q + H \frac{\partial^2 w}{\partial x^2} + \rho A \frac{\partial^2 w}{\partial t^2} = 0 \qquad (1)$$

Note here that M is the total bending moment present in the arch. Thus from standard beam theory

$$M = EI \frac{\partial^2 w}{\partial x^2} \qquad (2)$$

The end thrust is given by

$$H = H_o + \frac{EA}{L} \Delta L$$

where

$$\Delta L = \frac{1}{2}\int_{-L/2}^{L/2}\left[\left(\frac{\partial w_o}{\partial x}\right)^2 - \left(\frac{\partial w}{\partial x}\right)^2\right]dx - \delta$$

and δ is the deflection of the axial spring. Thus

$$H = H_o + \frac{EA}{2L}\int_{-L/2}^{L/2}\left[\left(\frac{\partial w_o}{\partial x}\right)^2 - \left(\frac{\partial w}{\partial x}\right)^2\right]dx - \frac{EA\delta}{L}$$

Also, if α represents the spring constant of the axial spring,

$$H = H_o + \alpha\delta$$

Combining these two expressions gives

$$\delta = \frac{EA}{2L(\alpha + EA/L)}\int_{-L/2}^{L/2}\left[\left(\frac{\partial w_o}{\partial x}\right)^2 - \left(\frac{\partial w}{\partial x}\right)^2\right]dx$$

and therefore

$$H = H_o + \frac{AE}{2L}\left[\frac{1}{1+EA/L\alpha}\right]\int_{-L/2}^{L/2}\left[\left(\frac{\partial w_o}{\partial x}\right)^2 - \left(\frac{\partial w}{\partial x}\right)^2\right]dx \qquad (3)$$

Substitution of (2) and (3) into (1) then give the final equation of motion

$$EI\frac{\partial^4 w}{\partial x^4} + \left\{H_o + \frac{AE}{2L}\left(\frac{1}{1+EA/L\alpha}\right)\int_{-L/2}^{L/2}\left[\left(\frac{\partial w_o}{\partial x}\right)^2 - \left(\frac{\partial w}{\partial x}\right)^2\right]dx\right\}\frac{\partial^2 w}{\partial x^2}$$

$$+ q + \rho A\frac{\partial^2 w}{\partial t^2} = 0 \qquad (4)$$

It may be noted that there is some difference between (4) and the equation of motion as it is usually presented in the literature (in particular, reference 1, where this equation was obtained for the first time). Usually, the term $-EI\ \partial^4 w_o/\partial x^4 - H_o\ \partial^2 w_o/\partial x^2$ would be added to the left-hand side of (4). However the arch under consideration is assumed to have obtained its shape as the result of the buckling of a flat strip. Thus for this case;

$$EI\ \frac{\partial^4 w_o}{\partial x^4} + H_o\ \frac{\partial^2 w_o}{\partial x^2} = 0$$

It will later be shown that, by utilizing an energy analysis to treat the case of buckling under an impulsive load, only the static equilibrium positions of the arch under zero load need be considered. Thus in (4), the time dependency vanishes, and $q = 0$. (4) then becomes

$$EI\ \frac{d^4 w}{dx^4} + H\ \frac{d^2 w}{dx^2} = 0 \qquad (5)$$

where H is given by (3).

The analysis from this point will be similar to that presented by Vahidi in reference 2.

First equations (5) and (3) are written in terms of nondimensional variables by making the following substitutions:

$$y = \frac{w}{2}\sqrt{\frac{A}{I}}, \qquad y_o = \frac{w_o}{2}\sqrt{\frac{A}{I}}$$

$$\xi = \frac{\pi x}{L} \qquad \beta^2 = \frac{L^2}{\pi^2 EI} H$$

$$S = \frac{L^2}{\pi^2 EI} Ho \qquad C = \frac{1}{1+EA/L\alpha}$$

(5) thus becomes

$$\frac{d^4y}{d\xi^4} + \beta^2 \frac{d^2y}{d\xi^2} = 0 \tag{6}$$

and (3) becomes

$$\beta^2 = S + \frac{2C}{\pi} \int_{-\pi/2}^{\pi/2} \left[\left(\frac{dy_o}{\partial\xi}\right)^2 - \left(\frac{dy}{d\xi}\right)^2 \right] d\xi \tag{7}$$

For a sinusoidal arch with the coordinate system as indicated in Figure 4a, $y_o = r \cos \xi$

Also, for the particular case under consideration, H_o is just equal to the first Euler buckling load for the strip, and therefore $S = 1$.

The solutions of (6) describe the equilibrium positions of the arch, and, for any equilibrium position, β will be a constant. If we thus assume β to have a known constant value, the solution to (6) may immediately be found to be:

$$y = A_1 \sin \beta \xi + A_2 \cos \beta \xi + A_3 \xi + A_4 \tag{8}$$

where A_1, A_2, A_3 and A_4 are constants to be determined from the boundary conditions.

For the case of an arch with rotational end restraints (spring constant = K), the boundary conditions in nondimensional form are:

$$y(-\tfrac{\pi}{2}) = y(\tfrac{\pi}{2}) = 0$$

$$K'(y_o' - y') + (y_o'' - y'') = 0 \qquad \text{at } \xi = \pi/2$$

$$K'(y_o' - y') - (y_o'' - y'') = 0 \qquad \text{at } \xi = -\pi/2$$

where $K' = \dfrac{KL}{\pi EI}$

These then give four equations for the four undetermined constants A_1, A_2, A_3 and A_4.

$$A_1 \sin\frac{\beta\pi}{2} + A_2 \cos\frac{\beta\pi}{2} + \frac{\pi A_3}{2} + A_4 = 0 \tag{9a}$$

$$-K'(r + A_1\beta\cos\frac{\beta\pi}{2} - A_2\beta\sin\frac{\beta\pi}{2} + A_3) + A_1\beta^2\sin\frac{\beta\pi}{2} + A_2\beta^2\cos\frac{\beta\pi}{2} = 0 \tag{9b}$$

$$-A_1\sin\frac{\beta\pi}{2} + A_2\cos\frac{\beta\pi}{2} - \frac{\pi}{2}A_3 + A_4 = 0 \tag{9c}$$

$$-K'(-r + A_1\beta\cos\frac{\beta\pi}{2} + A_2\beta\sin\frac{\beta\pi}{2} + A_3) + A_1\beta^2\sin\frac{\beta\pi}{2} - A_2\beta^2\cos\frac{\beta\pi}{2} = 0 \tag{9d}$$

Now subtract (9c) from (9a), and add (9b) to (9b). The result is

$$2A_1 \sin \frac{\beta\pi}{2} + \pi A_3 = 0 \tag{10a}$$

$$-2K'\beta A_1 \cos \frac{\beta\pi}{2} - 2K'A_3 + 2A_1\beta^2 \sin \frac{\beta\pi}{2} = 0 \tag{10b}$$

Similarly, add (9c) to (9a) and subtract (9d) from (9b) to obtain

$$A_2 \cos \frac{\beta\pi}{2} + A_4 = 0 \tag{11a}$$

$$A_2(K'\beta \sin \frac{\beta\pi}{2} + \beta^2 \cos \frac{\beta\pi}{2}) - K'r = 0 \tag{11b}$$

Note that (10a, 10b) contain only the antisymmetric components of the arch deformation, while (11a, 11b) contain only the symmetric components. Solving (11a, 11b) gives

$$A_2 = \frac{K'r}{K'\beta \sin \frac{\beta\pi}{2} + \cos \frac{\beta\pi}{2}} \tag{12a}$$

$$A_4 = -A_2 \cos \frac{\beta\pi}{2} \tag{12b}$$

Rewriting (10a, 10b),

$$A_1 \sin \frac{\beta\pi}{2} + \frac{\pi}{2} A_3 = 0 \tag{13a}$$

$$A_1(\beta^2 \sin \frac{\beta\pi}{2} - K'\beta \cos \frac{\beta\pi}{2}) - K'A_3 = 0 \tag{13b}$$

Two possibilities exist here.

i. $A_1 = A_3 = 0$, which implies that the deflected arch shape is symmetric.

ii. A_1, $A_3 \neq 0$, which implies that the determinant of the matrix of coefficients vanishes, i.e.

$$K' \sin\frac{\beta\pi}{2} + \frac{\pi}{2}(\beta^2 \sin\frac{\beta\pi}{2} - K'\beta \cos\frac{\beta\pi}{2}) = 0 \tag{14}$$

This equation is a transcendental equation for β. It is interesting to note that this equation always has solutions, even for the case $K' \to \infty$. In this instance, (14) becomes

$$\tan\frac{\beta\pi}{2} = \frac{\beta\pi}{2}$$

which does indeed have solutions. Note also that for A_1, $A_3 \neq 0$, we cannot yet obtain explicit representations for A_1 and A_3, but only a relation between the two. From (13a), this relation is

$$A_3 = \frac{2}{\pi} A_1 \sin\frac{\beta\pi}{2} \tag{15}$$

Recall we assumed at the start that β had some known constant value which, however, was not specified. Apparently, then, another relation is needed in order to completely determine the equilibrium states. This relation is supplied by requiring (7) to be satisfied. For if we substitute the expressions for y and y_o into (7), we obtain

$$\frac{1}{C}(\beta^2 - 1) - r^2 + \frac{2}{\pi} A_1^2 \beta(\frac{\beta\pi}{2} + \sin\frac{\beta\pi}{2}\cos\frac{\beta\pi}{2}) + \frac{2}{\pi} A_2^2 \beta(\frac{\beta\pi}{2} - \sin\frac{\beta\pi}{2}\cos\frac{\beta\pi}{2})$$
$$+ 2A_3^2 + \frac{8}{\pi} A_1 A_3 \sin\frac{\beta\pi}{2} = 0 \tag{16}$$

(16) is called the "constraint equation" by Vahidi. With the inclusion of (16), the problem is completely determined.

In the interest of clarity, the method of obtaining solutions for the separate cases $A_1 = A_3 = 0$ and $A_1, A_3 \neq 0$ will now be outlined.

i. $A_1 = A_3 = 0$ (symmetric case)

In this case the deflected equilibrium position is, from (8),

$$y = A_2 \cos \beta\xi + A_4 \tag{17}$$

where A_2 and A_4 are given by (12a) and (12b) respectively. Noting that A_2 and A_4 are functions of β and known arch parameters, (12a, 12b) may be substituted into (16) to obtain a transcendental equation which may then be solved for β. The roots of this equation may then be substituted into (17) to obtain expressions for the equilibrium positions of the arch.

ii. $A_1, A_3 \neq 0$ (antisymmetric case)

In this case (14) must be satisfied. (14) is another transcendental equation in β, the roots of which describe the equilibrium positions of the arch. Knowing the equilibrium values of β, A_2 and A_4 may be calculated. However, A_1 and A_3 are still indeterminant. Knowing β, we may use (15) and (16) to solve for A_1 and A_3. Putting (15) into (16) gives

$$D_2 A_1^2 + D_1 = 0 \tag{18}$$

where

$$D_2 = \frac{2\beta}{\pi}\left(\frac{\beta\pi}{2} + \sin\frac{\beta\pi}{2}\cos\frac{\beta\pi}{2}\right) - \frac{8}{\pi^2}\sin^2\frac{\beta\pi}{2} \tag{19a}$$

$$D_1 = \frac{1}{C}(\beta^2 - 1) - r^2 + \frac{2}{\pi}A_2^2\,\beta\left(\frac{\beta\pi}{2} - \sin\frac{\beta\pi}{2}\cos\frac{\beta\pi}{2}\right) \tag{19b}$$

Thus

$$A_1 = \pm\sqrt{-\frac{D_1}{D_2}} \tag{20}$$

The $\pm$ sign simply means that no antisymmetric orientation is preferred. Note there exists a possibility that (20) may possess no real roots. This possibility will be discussed later.

A digital computer program was written to solve the two transcendental equations and to calculate the deflected equilibrium positions for both the symmetric and antisymmetric cases. A plot of some of the lower equilibrium values of β vs. K' obtained by this program is given in Figure 5.

B. Stability under Impulsive Load

To characterize the stability of the arch under an impulsive load, the strain energy present in any equilibrium position must first be calculated. The difference in strain energy from the undeformed state is given by

$$\bar{U} = \frac{L}{2AE}(H^2 - H_o^2) + \frac{1}{2} EI \int_{-L/2}^{L/2} \left[\left(\frac{d^2 w}{dx^2}\right)^2 - \left(\frac{d^2 w_o}{dx^2}\right)^2 \right] dx +$$

$$K/2 \left\{ \left[\frac{d(w-w_o)}{dx} \right]^2_{x=-L/2} + \left[\frac{d(w-w_o)}{dx} \right]^2_{x=L/2} \right\} + \frac{1}{2}\alpha \left[(\delta + \Delta)^2 - \Delta^2 \right] \tag{21}$$

where

$$\delta = \frac{EA}{2L(\alpha + EA/L)} \int_{-L/2}^{L/2} \left[\left(\frac{dw_o}{dx}\right)^2 - \left(\frac{dw}{dx}\right)^2 \right] dx$$

$$\Delta = H_o \alpha \tag{22}$$

Now define a nondimensional energy by

$$U = \frac{AL^3}{\pi^4 EI^2} \bar{U} \tag{23}$$

Substituting (22) into (21) and using (23) gives

$$U = \frac{1}{2}(\beta^2 - 1) + \frac{2}{\pi} \int_{-\pi/2}^{\pi/2} \left[\left(\frac{d^2 y}{d\xi^2}\right) - \left(\frac{d^2 y_o}{d\xi^2}\right)^2 \right] d\xi + \frac{2K'}{\pi} \left\{ \left[\frac{d(y-y_o)}{d\xi} \right]^2_{\xi=-\pi/2} \right.$$

$$\left. + \left[\frac{d(y-y_o)}{d\xi} \right]^2_{\xi=\pi/2} \right\} + \frac{8L\alpha}{\pi^2 EA} \left[\frac{EA/L}{2(\alpha + EA/L)} \right]^2 \left\{ \int_{-\pi/2}^{\pi/2} \left[\left(\frac{dy_o}{d\xi}\right)^2 - \left(\frac{dy}{d\xi}\right)^2 \right] d\xi \right\}^2$$

$$+ \frac{4}{\pi} \left[\frac{EA/L}{2(\alpha + EA/L)} \right] \left\{ \int_{-\pi/2}^{\pi/2} \left[\left(\frac{dy_o}{d\xi}\right)^2 - \left(\frac{dy}{d\xi}\right)^2 \right] d\xi \right\} \tag{24}$$

Now write

$$U = U_1 + U_2 + U_3 + U_4 \tag{25}$$

Here

$$U_1 = \frac{1}{2}(\beta^4 - 1) \tag{26}$$

$$U_2 = \frac{2}{\pi}\int_{-\pi/2}^{\pi/2}\left[\left(\frac{d^2y}{d\xi^2}\right)^2 - \left(\frac{d^2y_o}{d\xi^2}\right)^2\right] d\xi$$

$$= \frac{A_1^2\beta^3}{\pi}\left[\beta\pi - \sin\beta\pi\right] + \frac{A_2^2\beta^3}{\pi}\left[\beta\pi + \sin\beta\pi\right] - r^2 \tag{27}$$

by using (8) and the relation $y_o = r\cos\xi$

$$U_3 = \frac{2K'}{\pi}\left\{\left[\frac{d(y-y_o)}{d\xi}\right]^2_{\xi=-\pi/2} + \left[\frac{d(y-y_o)}{d\xi}\right]^2_{\xi=\pi/2}\right\}$$

$$= \frac{2K'}{\pi}\left[2A_1^2\beta^2\cos^2\frac{\beta\pi}{2} + 2A_2^2\beta^2\sin^2\frac{\beta\pi}{2} + 2A_3^2\right. \tag{28}$$

$$\left. + 2r^2 + 4A_1A_3\beta\cos\frac{\beta\pi}{2} - 4A_2\beta r\sin\frac{\beta\pi}{2}\right]$$

$$U_4 = \frac{8L\alpha}{\pi^2 EA}\left[\frac{EA/L}{2(\alpha + EA/L)}\right]^2\left\{\int_{-\pi/2}^{\pi/2}\left[\left(\frac{dy_o}{d\xi}\right)^2 - \left(\frac{dy}{d\xi}\right)^2\right] d\xi\right\}^2 +$$

$$\frac{4}{\pi}\left[\frac{EA/L}{2(\alpha+EA/L)}\right]\left\{\int_{-\pi/2}^{\pi/2}\left[\left(\frac{dy_o}{d\xi}\right)^2 - \left(\frac{dy}{d\xi}\right)^2\right] d\xi\right\}$$

or

$$U_4 = \frac{2L\alpha}{EA}\left[\frac{EA/L}{2(x + EA/L)}\right]^2\left(\frac{\beta^2-1}{C}\right)^2 + \frac{EA/L}{(\alpha+ EA/L)}\left(\frac{\beta^2-1}{C}\right) \tag{29}$$

Now that an expression for the strain energy has been derived, we may apply Hsu's criterion to the case of impulsive loading to determine the stability of the arch.

Consider a uniformly distributed impulsive load given by

$$q(t) = B\delta(t) \tag{30}$$

The initial velocity of the arch will then be

$$\dot{w} = B/\rho A$$

and its initial energy is

$$\bar{V} = \frac{1}{2}\frac{B^2 L}{\rho A} \tag{31}$$

Now Hsu's stability criterion is that $\bar{V}$ be less than some critical value $\bar{V}^*$. If $\bar{V} > \bar{V}^*$, then the possibility of dynamic snap through exists.

In order to determine $\bar{V}^*$ for the arch, consider Figure 6, which depicts an energy surface for the arch with no applied load. Here q_1 represents some symmetric component of the deflected shape, and q_2 some antisymmetric component. The contours represent equi-strain energy curves. A diagram of this sort for the arch was first presented by Hoff and Bruce in reference 4.

From the condition that equilibrium positions correspond to an extremum on the energy surface, we see that, within the simplified representation of the diagram, there are only four equilibrium positions available apart from the initial position (actually there may be more, depending on the initial arch rise, but these have no meaning in

the present discussion). The two positions with q_2 components are saddle points and are thus unstable. One of the positions on the q_1 axis is at the top of a "hill" and is unstable; the other is at the bottom of a depression and is a stable equilibrium position.

Now it is known that no matter how many equilibrium positions the arch possesses under zero load, there may exist only one stable position apart from the initial position. This is the "snapped through" position, in which the arch undergoes a reversal of curvature along most of its length. This position is made up of symmetric deflection components only, and may be identified with the depression in the energy surface.

We may consider the arch to describe a trajectory over the energy surface in $q_1 - q_2$ space. Now the effect of the impulsive load is to impart an initial energy to the arch. If enough energy is imparted to the arch, the trajectory will be able to cross over the rise in the energy surface separating the original unloaded equilibrium position from the snapped through equilibrium position. When this happens, dynamic buckling is said to have occurred. However, if the arch does not have enough energy to cross the rise, the trajectory will always remain in the vicinity of the original position.

From the definition of $\bar{V}^*$ as that initial energy above which dynamic buckling may occur, it is easy to see that $\bar{V}^*$ is just equal to the energy associated with the saddle points, as these are the points having the lowest energies on the rise separating the two stable equilibrium positions. It is also easy to see how this satisfies the definition of dynamic buckling given in the Introduction. Suppose the arch follows

a trajectory which passes through one of the saddle points. Then if the arch has an initial energy $\bar{V}^*$, the trajectory will eventually come to rest at the saddle point in unstable equilibrium, taking an infinitely long time to do so. However if the arch has an initial energy $\bar{V} = \bar{V}^* + \Delta\bar{V}$, then it will have sufficient energy so that the trajectory will cross the saddle point and proceed down the other side of the rise. Thus an infinitesimal increase in load (and thus initial energy) has produced a finite increase in displacement.

If the trajectory was to pass over some part of the rise other than the saddle points, more energy would be required than that necessary to cross at the saddle points. Thus $\bar{V}^*$ is a necessary condition for dynamic buckling.

It should be noted that, for Hsu's criterion to be applicable, there must exist at least one stable equilibrium position other than the undeflected position. If the undeflected position is the only stable equilibrium position, then all trajectories which start out from this point on the energy surface will eventually return to the same point. Thus dynamic buckling in the sense of Hsu is not possible. This, of course, implicitly assumes that the arch will never come to rest in an unstable equilibrium position.

A plot of strain energy vs. K' is given in Figure 7, for $r = 39.8$ for the first three equilibrium positions. It can be seen that the first symmetric position has the lowest energy. This corresponds to the stable snapped through equilibrium position. The next highest energy is associated with the first antisymmetric position, which corresponds to the saddle points, or $\bar{V}^*$.

C. Effect of Increasing Torsional Spring Stiffness

It was stated previously that, in order for Hsu's stability criterion to be applicable, the arch must possess at least one other stable equilibrium position other than the original unloaded position. If such is not the case, then the arch must always be stable in the sense of Hsu.

Now the simply supported arch is known to have a stable equilibrium position other than the original unloaded position. This is the snapped through position. Contrariwise, it has been shown by Vahidi (Ref. 7) and confirmed experimentally by Cheung (Ref. 6) that the clamped arch has no stable equilibrium position other than the original position. This then suggests that there exists some critical value of rotational spring constant above which the arch possesses only one stable equilibrium position, the undeflected one. Above this critical value, dynamic buckling in the mathematical sense may not occur.

It is suspected, therefore, that at some point the first symmetric (snapped through) position loses its stability and becomes unstable. The mechanism causing this to occur may be deduced by considering Figure 7. With increasing spring stiffness, the strain energy curves for the first symmetric and first antisymmetric equilibrium positions tend to run together until they merge. By then looking at the energy surface in Figure 6, it can be seen that this implies that the two saddle points are merging in along the q_2 axis towards the depression representing the first symmetric position. When this merger becomes complete, the first symmetric position will become a saddle point, and will thus lose its stability.

At this point, the antisymmetric equilibrium positions will have ceased to exist. In order to determine the value of rotational spring constant at which this occurs, consider equation (20), which is

$$A_1 = \pm \sqrt{-\frac{D_1}{D_2}}$$

where

$$D_1 = \frac{1}{C}(\beta^2 - 1) - r^2 + \frac{2}{\pi} A_2^2 \beta(\frac{\beta\pi}{2} - \sin\frac{\beta\pi}{2}\cos\frac{\beta\pi}{2})$$

$$D_2 = \frac{2\beta}{\pi}(\frac{\beta\pi}{2} + \sin\frac{\beta\pi}{2}\cos\frac{\beta\pi}{2}) - \frac{8}{\pi^2}\sin^2\frac{\beta\pi}{2}$$

β is assumed to have been determined from equation (14).

Consider first the expression for D_2. From equation (14) and Figure 5 it can be seen that the lowest possible value of β for antisymmetry is $\beta = 2$. This simply corresponds to an end thrust equal to the second Euler buckling load for the strip when $K' = 0$. Thus D_2 will always be positive.

Now consider the expression for D_1. If antisymmetric equilibrium positions are to exist, D_1 must be negative. For arches with any appreciable rise, r^2 will be relatively large (approximately 1600 for the arch used in the experiment). Thus for K' small enough, D_1 will indeed be negative, and antisymmetric solutions will exist.

The value of K' at which antisymmetric positions will cease to exist may be found by setting $D_1 = 0$. Thus

$$\frac{1}{C}(\beta^2 - 1) - r^2 + \frac{2}{\pi} A_2^2 \beta(\frac{\beta\pi}{2} - \sin\frac{\beta\pi}{2}\cos\frac{\beta\pi}{2}) = 0$$

Substituting for A_2 from equation (12a) gives

$$\frac{1}{C}(\beta^2-1) - r^2 + \frac{2\beta(K'r)^2(\frac{\beta\pi}{2} - \sin\frac{\beta\pi}{2}\cos\frac{\beta\pi}{2})}{\pi(K'\beta\sin\frac{\beta\pi}{2} + \beta^2\cos\frac{\beta\pi}{2})^2} = 0 \qquad (32)$$

This equation can be put in terms of β alone by solving equation (14) for K'. Thus

$$K' = \frac{\frac{\pi\beta^2}{2}\sin\frac{\beta\pi}{2}}{\frac{\pi\beta}{2}\cos\frac{\beta\pi}{2} - \sin\frac{\beta\pi}{2}} \qquad (33)$$

Substituting (33) into (32) gives a transcendental equation for β. The lowest root of this equation will then give the critical value of K', when substituted back into (33). The lowest value of β must be used, as this root will be the last to disappear with increasing K'. This may be realized by considering the equation for D_2.

The fact that only the original position exists for the clamped arch implies that all symmetric positions will likewise disappear with increasing K'. When this occurs, equation (16) will no longer possess any real roots.

IV. RESULTS

As stated previously, the arch employed in the experimental part of the work had a central rise of 23/32 in. It was 15 in. long, 1 in. wide, and 1/32 in. thick. Four different stiffnesses of torsion rods were used, having experimentally measured spring constants of $K = 85.0$, 75.0, 48.8 and 22.5 in-lbs/rad, corresponding to non-dimensional values of $K' = 5.29$, 4.67, 3.04 and 1.40 respectively. An axial spring with a spring constant of 16,600 lbs/in was also included.

1. Deflection Shapes

In order to see how closely the theory predicted the static equilibrium arch shapes, measurements were made of the vertical deflection of the arch in the snapped through position. The measurements were made at a number of stations near the arch center using a pair of dividers. The results are presented in Figures 8a-d. It can be seen that in most cases the agreement between the theoretically predicted deflection curves and the experimentally measured values is quite good.

Along with this, an attempt was made to determine experimentally that critical value of rotational spring constant above which a stable snapped through position could not exist. It was found that for $K = 100$ in-lbs/rad, the arch would not remain in the snapped through position, but tended to spring back into its original shape when released. Since a stable snapped through position was achieved for $K = 85.0$ in-lbs/rad, the critical value is surmised to lay somewhere between $K = 85$-100 in-lbs/rad.

Using equations (32), (33) the theoretical critical value was calculated. This gave K = 633 in-lbs/rad. The wide discrepancy between the theoretical and experimental values will be discussed later.

2. Uniform Impulsive Loading

The impulsive loading experiments were conducted by laying 15" strips of explosive-sprayed Mylar onto the arch to be loaded. These were then ignited with a zenon flash tube, as described previously. Plots of arch central deflection vs. total impulse applied to the arch are given in Figures 9a-d and 10. It may be observed that the experimental points exhibit a good deal of scatter. This is in part due to the inaccuracies inherent in the deflection measuring apparatus. Another source of error arises from the fact that the arch central deflection may not in all cases give a good indication of the magnitude of the arch response. Cheung (Ref. 6), for example, uses as a measure of arch response the area between the deformed and undeformed arch shapes.

It may be seen from the plots, however, that for some rather narrow range of impulse level, there is a large jump in arch central deflection. This type of response is typical of the dynamic buckling phenomenon.

In order to make a comparison with theory, dynamic buckling was said to have occurred experimentally when the central arch deflection reached a value of 0.6 in. Corresponding values of total impulse were then read from Figure 10. These are plotted as total initial energy imparted to the arch in Figure 12. Also plotted here

are the strain energies corresponding to the first three equilibrium positions (those having the lowest values of β). Theoretically, the curve corresponding to the first antisymmetric position represents a lower bound on the initial energy required for buckling. It can be seen that the experimental values are in fact quite a bit higher than this curve.

3. Experiments with Nonuniform Loadings

In addition to conducting tests with uniformly-distributed impulsive loadings, several experiments were made with nonuniform loadings. Instead of using 15 in. strips of explosive which covered the length of the arch, shorter 4 in. strips were used which loaded only a portion of the arch length.

For the first of these tests, the 4 in. strips were placed along the central section of an arch having $K = 48.8$ in-lbs/rad. The deflection response vs. total applied impulse is plotted in Figure 11, along with the results for the same K using 15 in. strips. It may be seen that much less total impulse was necessary to buckle the arch with the 4 in. strip than with the 15 in. strip. Again, a value of critical impulse was obtained from Figure 11, converted to initial arch energy by means of equations (30) and (31), and plotted in Figure 12. It can be seen that this value is much closer to the theoretically predicted lower bound than those values obtained by uniform loadings.

For the second test, the drill chucks holding the torsion rods were loosened so that the ends of the arch were free to rotate. In this way, it was hoped to approximate simply supported boundary conditions. The 4 in. strips were then placed alternatively along the central section

of the arch, or at one-quarter of the length from the end of the arch. The responses are plotted in Figure 12. It can be seen that the critical impulse for the arch loaded along one side is somewhat less than for the arch loaded in the center. This is to be expected from theoretical considerations, since it was shown previously that an arch required less initial energy to buckle in an antisymmetric shape than a symmetric shape. Loading the arch along one side apparently tends to drive the arch along a more antisymmetric trajectory than would be the case if the arch were centrally loaded.

As before, the approximate critical values of total impulse are plotted as initial energy imparted to the arch in Figure 12.

V. DISCUSSION

A theoretical and experimental investigation of the buckling of a shallow arch under an impulsive load has been carried out. Elastic rotational restraints were attached to the ends of the arch and an axial spring was included.

1. Deflection Shapes

From the rather good agreement between the theoretically predicted and experimentally measured deflection shapes (Figures 8a-d), it must be concluded that the static equilibrium positions of the unloaded arch are well characterized by the analysis presented in Section III.

An experiment was performed to determine that critical value of rotational spring constant above which stable snapped through positions ceased to exist. This value was found to lie somewhere in the range $K = 85\text{-}100$ in-lbs/rad. On the other hand, a theoretical analysis predicted a critical value of $K = 633$ in-lbs/rad. The wide discrepancy between these two values may be explained by considering Figure 7. It is observed that although the strain energy curves for the first symmetric and first antisymmetric positions merge into one another, they do so very slowly. Consequently there exists a considerable range of K for which these two curves lie quite closely together.

The first symmetric position corresponds to the stable snapped through position, and the first antisymmetric position is unstable. Thinking in terms of energy surfaces, this means that the depression in the surface containing the first symmetric position is very shallow.

Thus any small disturbance may suffice to jar the arch from this depression and into an unstable configuration. It goes without saying that the physical world is full of such disturbances. Therefore, the stability of the snapped through equilibrium position will practically exist only for much smaller values of rotational spring constant than would be indicated theoretically. Also, and possibly more importantly, the arch is an imperfect physical structure, and this will also reduce the critical value of rotational spring constant.

It was found that the inclusion of an axial spring in the theoretical analysis affected the equilibrium positions and the strain energy of these positions to only a negligible extent. The reason for this may be made clear by considering equation (16). The effect of the axial spring enters only through the first term in the equation. For the axial spring constant of 16,600 lbs-in, C is approximately equal to 0.2. Thus for low values of β, the first term is completely dominated by the r^2 term, which is approximately 1,600. The axial spring term similarly plays little part in the strain energy expression. The effect of the axial spring will only be felt for very soft axial springs or for low initial arch rises.

2. Uniform Impulsive Loading

An arch with different values of rotational spring constant was subjected to a series of uniformly distributed impulsive loadings. The response curves are plotted together in Figures 9a-d and 10. Increasing the value of the rotational spring constant is seen to have only a slight effect on the critical impulse required for buckling. Generally,

however, the greater the spring constant, the higher the level of impulse required for buckling.

Also, no significant change in the shape of the response curve can be noted with increasing spring constant. No experiments were conducted using rotational spring constants for which stable snapped through positions could not be achieved. Cheung, however, in reference 6 presented response curves for a clamped arch under a uniform impulsive load. The shape of these curves are somewhat flatter than those in Figure 10, but there is otherwise no qualitative difference. Cheung's curves similarly demonstrate a significant increase in deflection for a relatively small increase of applied impulse, which is a characteristic of the dynamic buckling phenomenon. This is an interesting result in view of the fact that the clamped arch cannot exhibit dynamic buckling in the mathematical sense of Hsu. However, since a "dynamic buckling-type" behavior is exhibited by the clamped arch, for which $K \rightarrow \infty$, it is not surprising that the response curves should show little variance for values of K which are relatively close together.

It should additionally be noted that the use of Hsu's criterion provides a very conservative lower bound on the critical impulse needed for buckling. In actuality, buckling occurred at an impulse level approximately three times as great as indicated by the lower bound.

3. Nonuniform Loading

For the first of these experiments, 4 in. explosive strips were placed on the central portion of an arch with rotational springs having

K = 48.8 in-lbs/rad. A significant reduction in the total impulse necessary to buckle the arch was noted. A possible explanation is that loading the arch along its central portion only tends to drive the arch through the second symmetric equilibrium position. The second symmetric position is comparable to the shape of a column under the third Euler buckling load, that is, one and one-half sine waves symmetric about the arch center. It can be seen from Figure 7 that for K' = 3.04, the second symmetric position has only a slightly higher energy than the first antisymmetric position, which represents a lower bound on initial energy necessary for buckling. Thus, in essence, the trajectory of the arch over the energy surface was "aimed" in such a manner as to reduce the initial energy required for buckling.

Another experiment of this type was carried out using approximate simple support boundary conditions. The reason for this was that at K = 0, the strain energy curves for the first antisymmetric and the second symmetric equilibriumpositions show their greatest difference in magnitude. Theoretically, if one could "aim" the arch trajectory through the second symmetric position and then through the first symmetric position, the arch aimed through the symmetric position should have the higher buckling load.

This was attempted experimentally by loading the arch with 4 in. strips first in its central portion to try to drive it through the second symmetric position. Then the arch was loaded along one side to try to drive it through the first antisymmetric position, which looks

something like a full sine wave. A reduction in buckling load for the off-center loadings was indeed noticed.

REFERENCES

1. Fung, Y. C. and Kaplan, A.: "Buckling of Low Arches or Curved Beams of Small Curvature", NACA TN 2840, (Nov. 1952).
2. Vahidi, B.: "Static and Dynamic Snap Through of Elastic, Shallow Arches", TR No. 10, University of California, San Diego, (March 1968).
3. Hsu, C. S.: "On Dynamic Stability of Elastic Bodies with Prescribed Initial Conditions", Int. J. Eng. Science, Vol. 4, (1966).
4. Hoff, N. J. and Bruce, V. G.: "Dynamic Analysis of the Buckling of Laterally Loaded Flat Arches", J. Math. Phys., Vol. 32, (1954).
5. Humphreys, J. S.: "On Dynamic Snap-Buckling of Shallow Arches", AIAA Journal, Vol. 4, No. 5, (May 1966).
6. Cheung, M. C.: "The Static and Dynamic Stability of Clamped Shallow Circular Arches", Ph. D. Dissertation, Aeronautics Department, California Institute of Technology, (June 1969).
7. Vahidi, B.: "Non-Existence of Snap Through for Clamped Shallow Elastic Arches Subjected to Impulsive Load", TR No. 8, University of California, San Diego, (March 1968).
8. Nevill, G. E. and Hoese, F. O.: "Impulsive Loading Using Sprayed Silver Acetylide-Silver Nitrate", Experimental Mechanics, (Sept. 1965).
9. Hoese, F. O.; Langner, C. G. and Baker, W. E.: "Simultaneous Initiation over Large Areas of a Spray Deposited Explosive", Experimental Mechanics, (Sept. 1968).

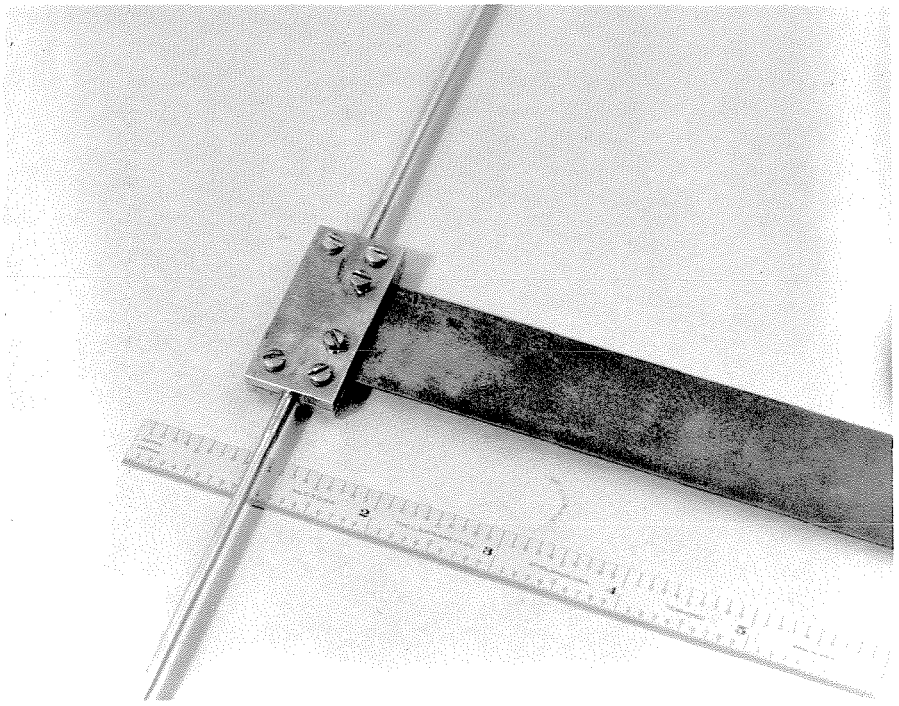

FIG. 1 ARCH END FIXTURE

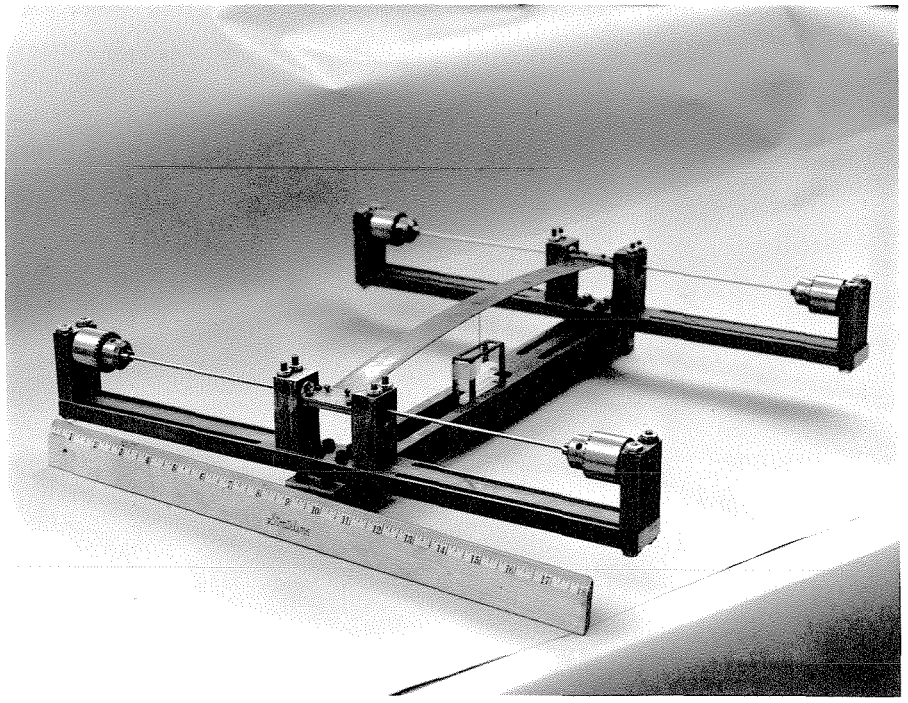

FIG. 2a COMPLETE ARCH FRAME

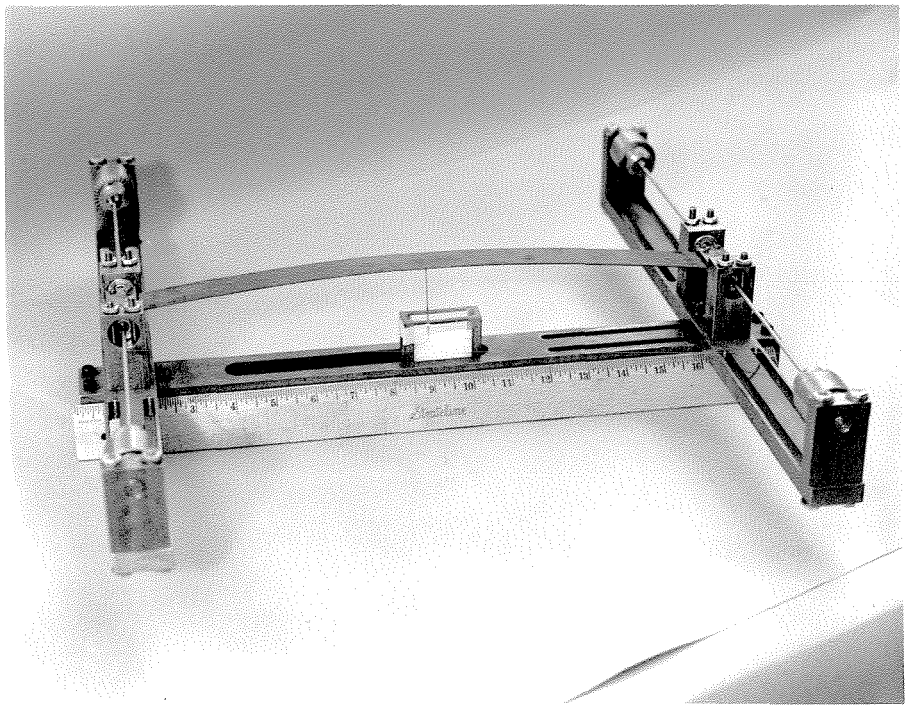

FIG. 2b COMPLETE ARCH FRAME

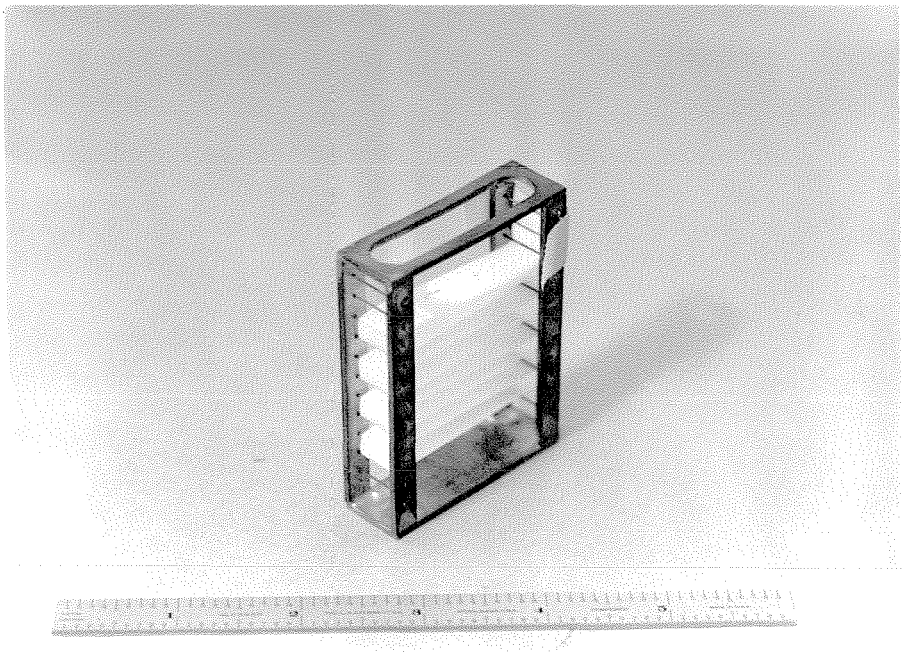

FIG. 3 TISSUE FRAME

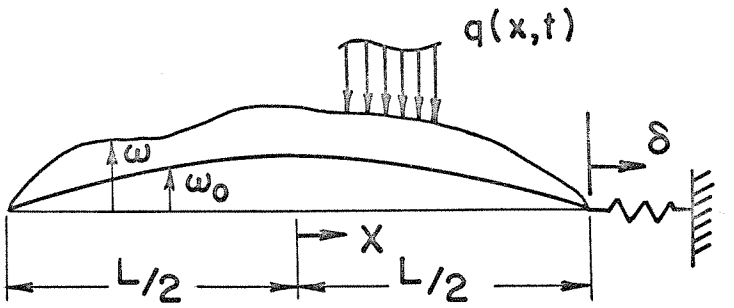

FIG. 4a ARCH GEOMETRY

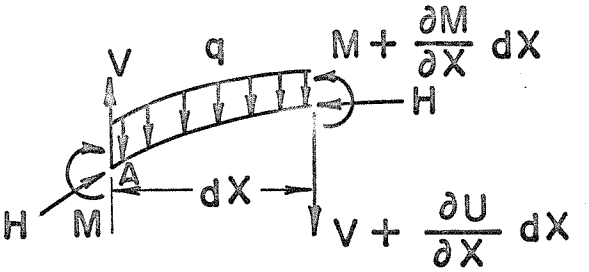

FIG. 4b DIFFERENTIAL ARCH ELEMENT

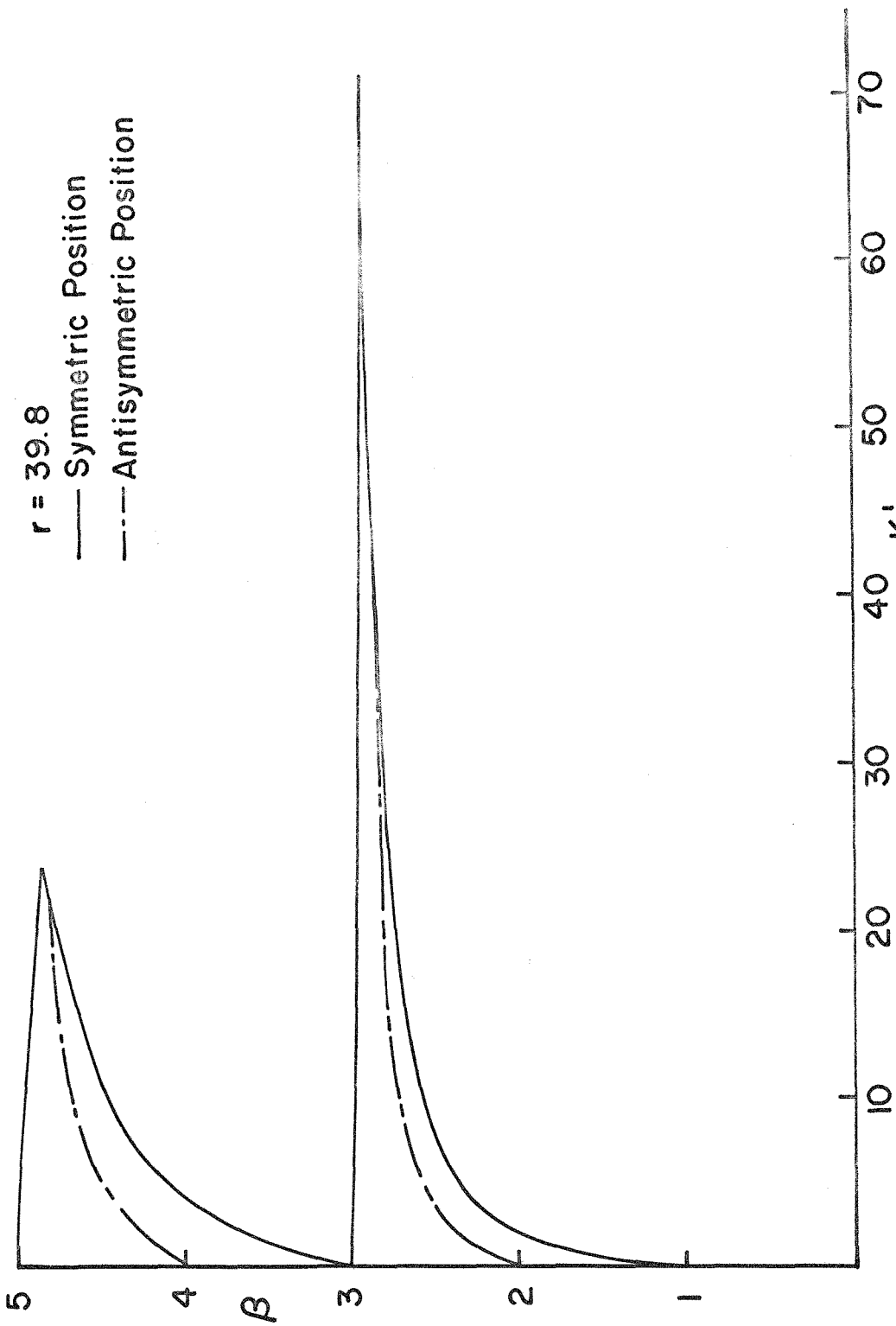

FIG. 5 β vs. NON-DIMENSIONAL SPRING CONSTANT

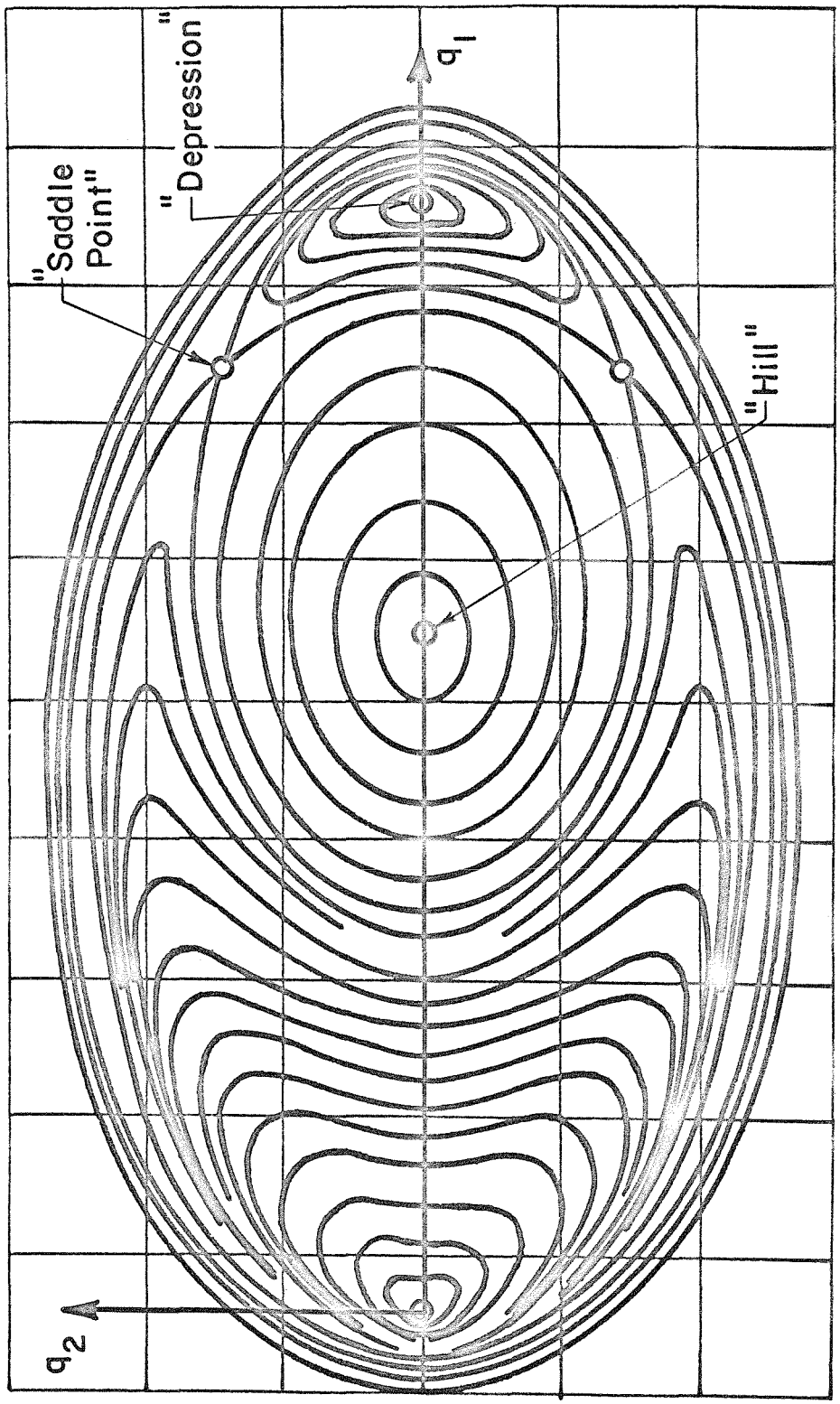

FIG. 6 ENERGY SURFACE (from Ref. 4)

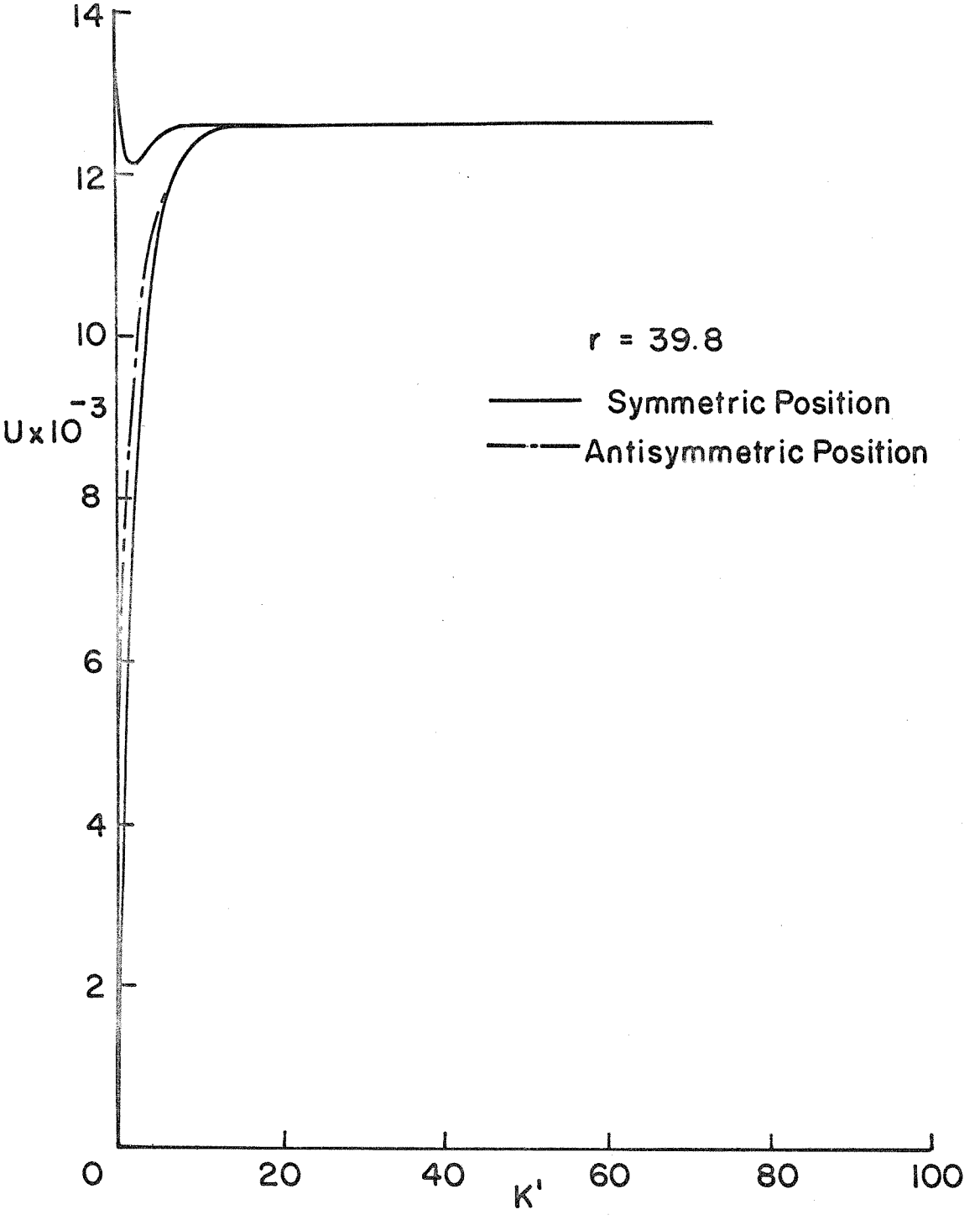

FIG.7 STRAIN ENERGY vs. K'

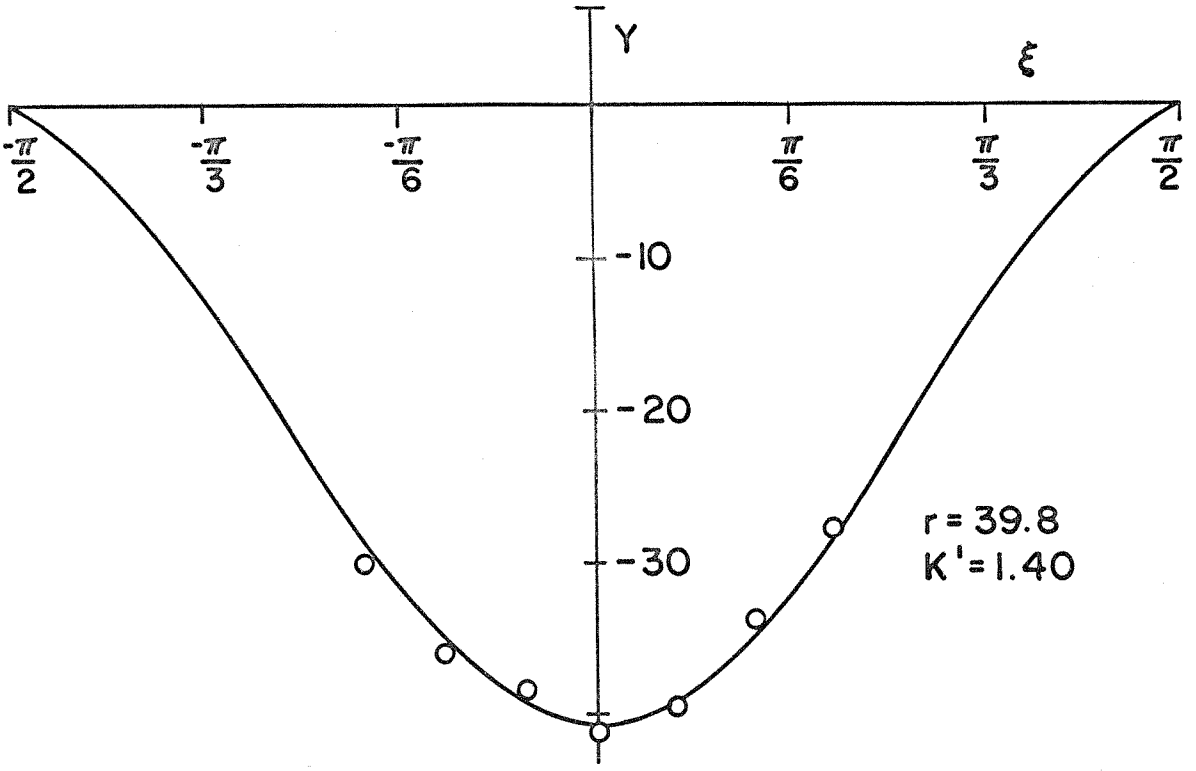

FIG. 8 a

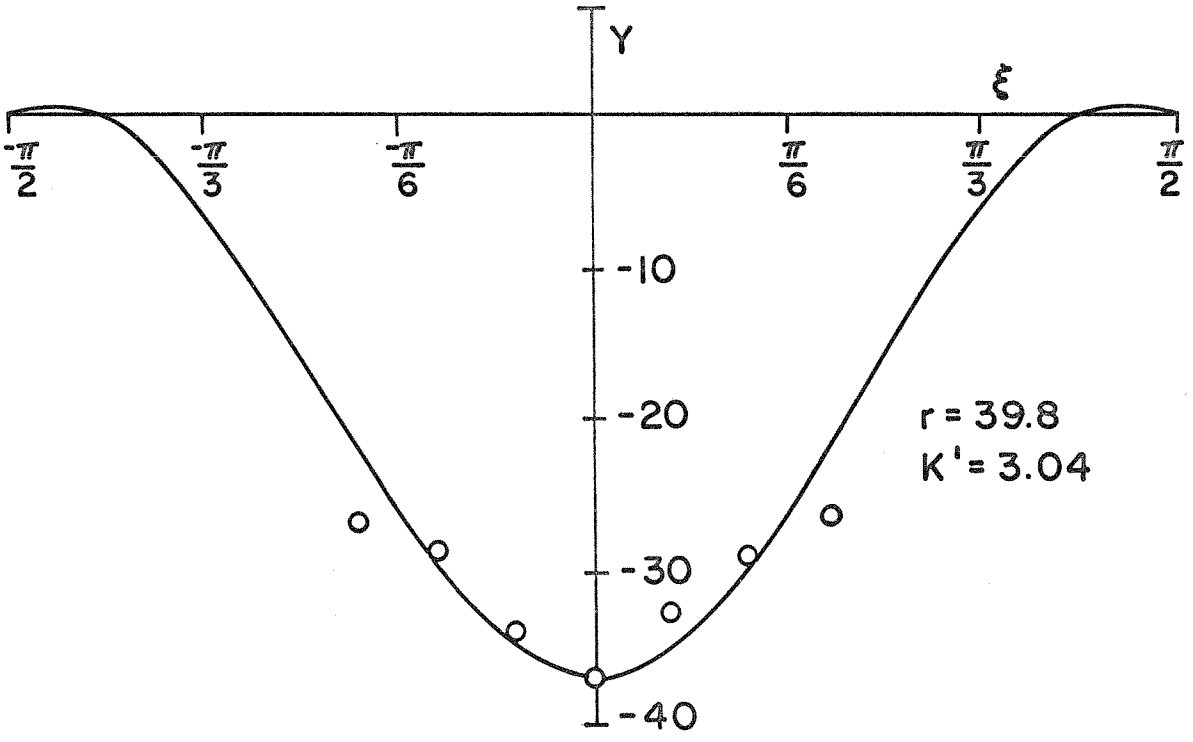

FIG. 8 b CALCULATED AND MEASURED DEFLECTION SHAPES

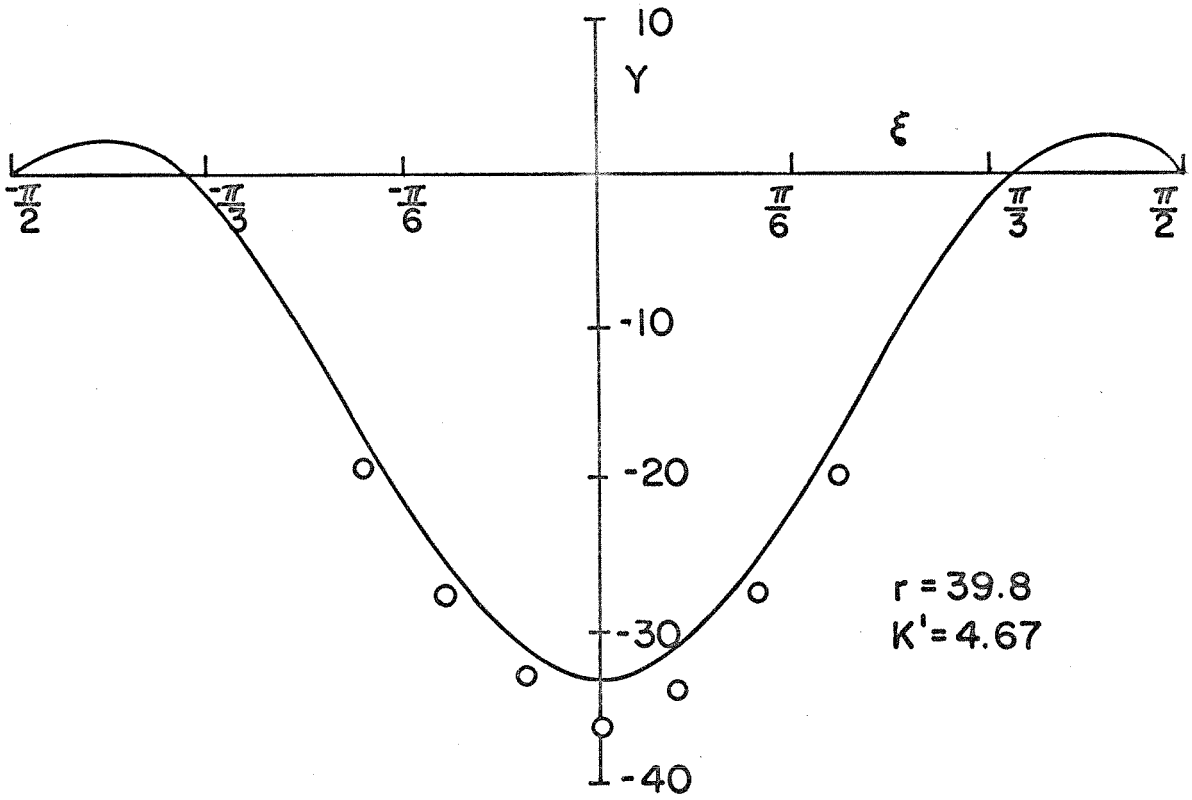

FIG. 8c

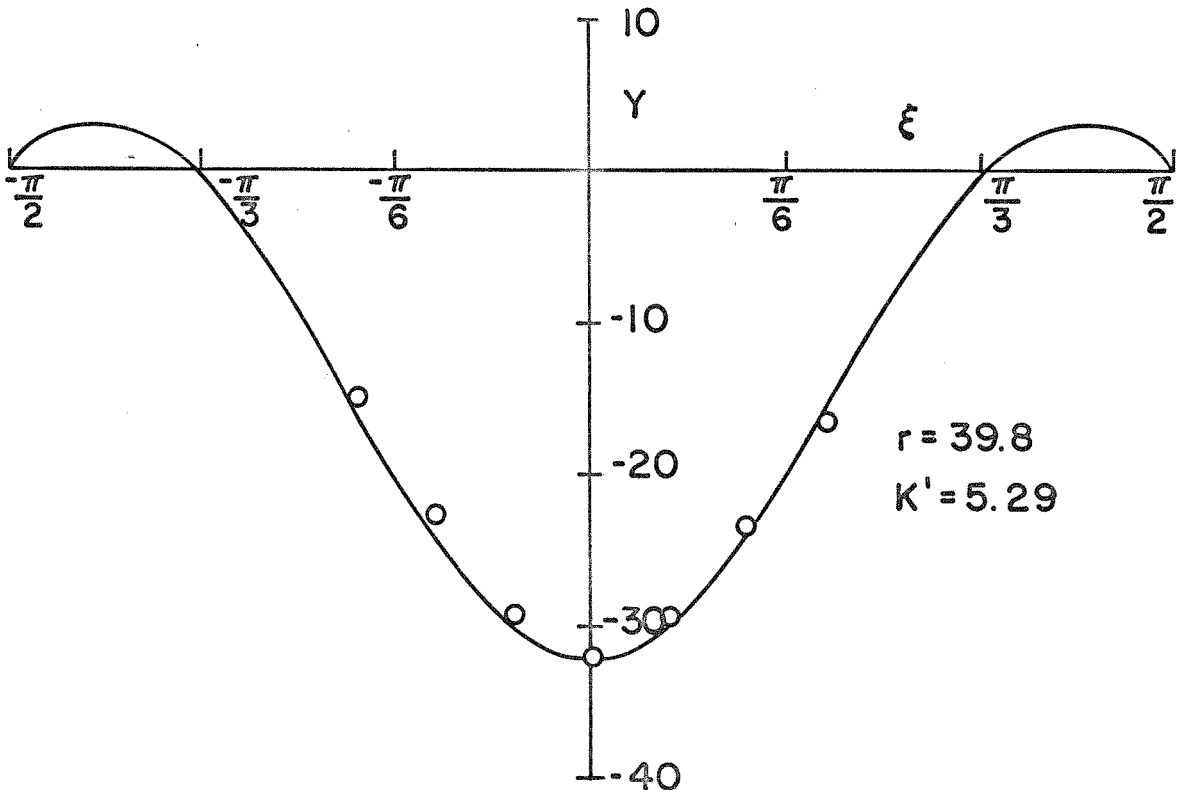

FIG. 8 d CALCULATED AND MEASURED DEFLECTION SHAPES

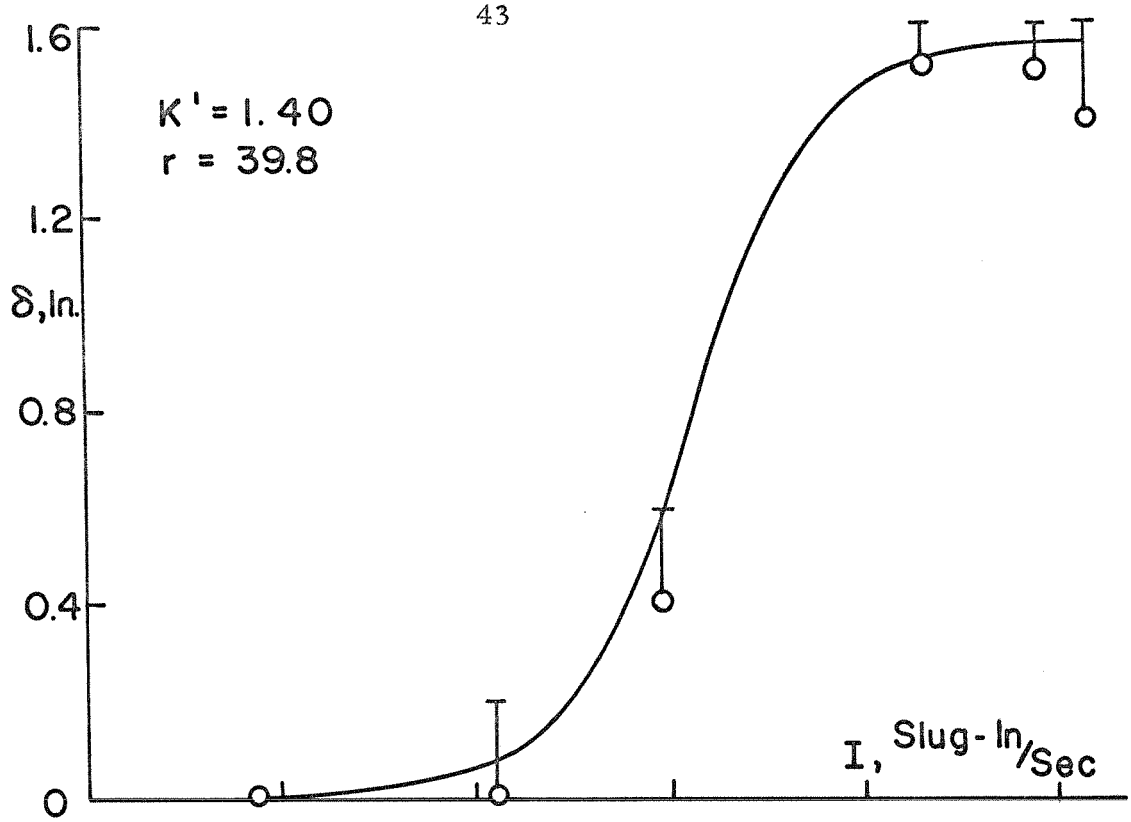

FIG. 9 a

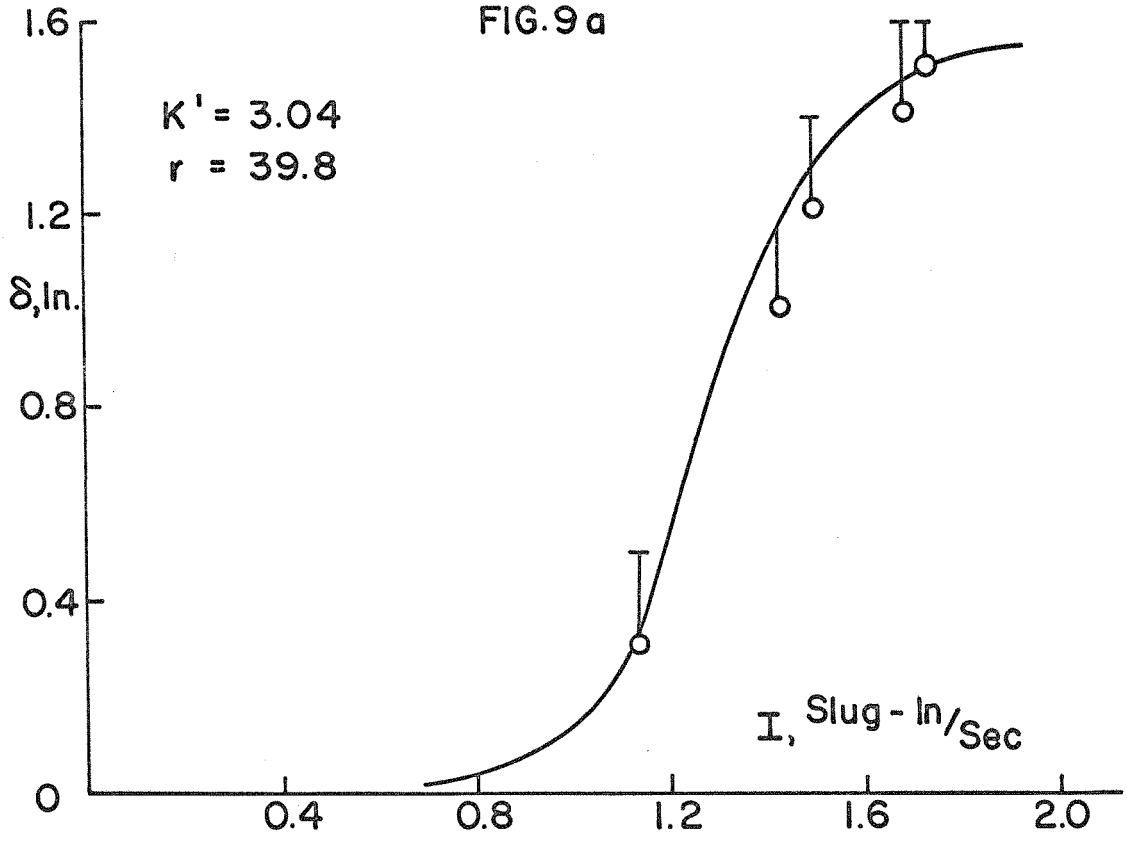

FIG. 9 b ARCH RESPONSE

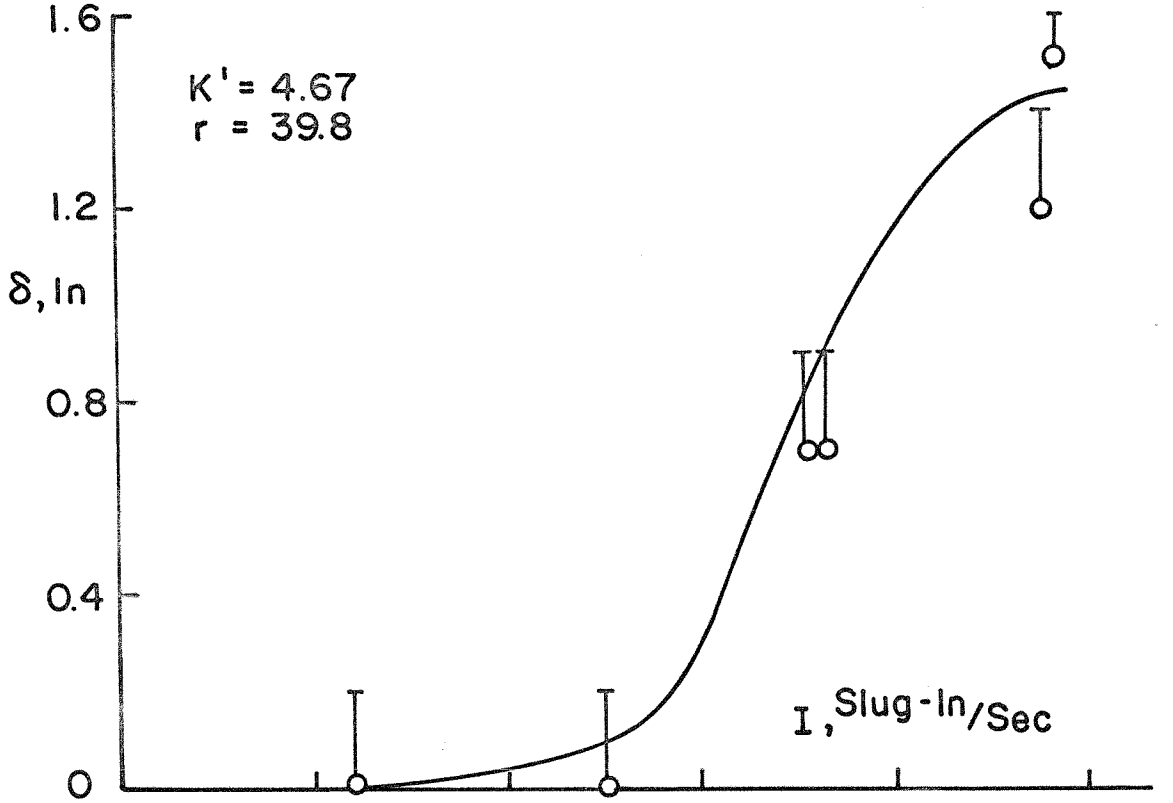

FIG. 9c

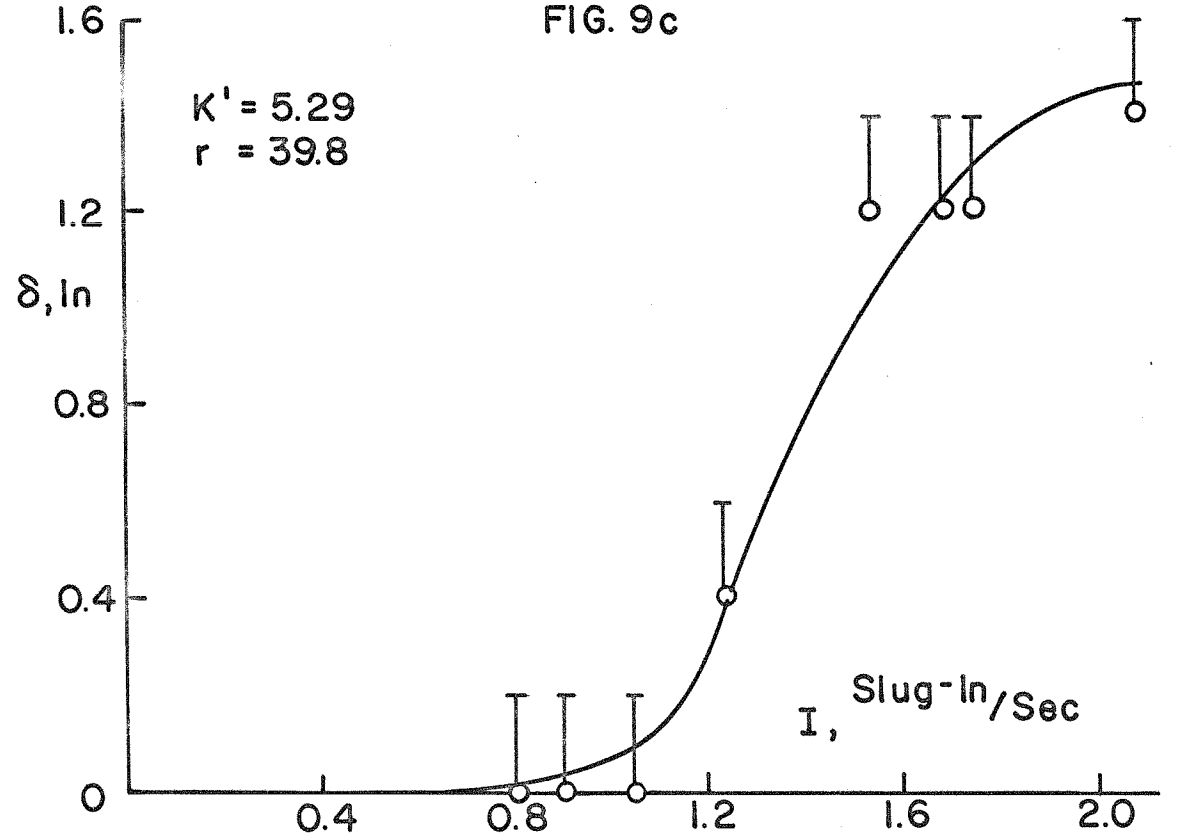

FIG. 9d ARCH RESPONSE

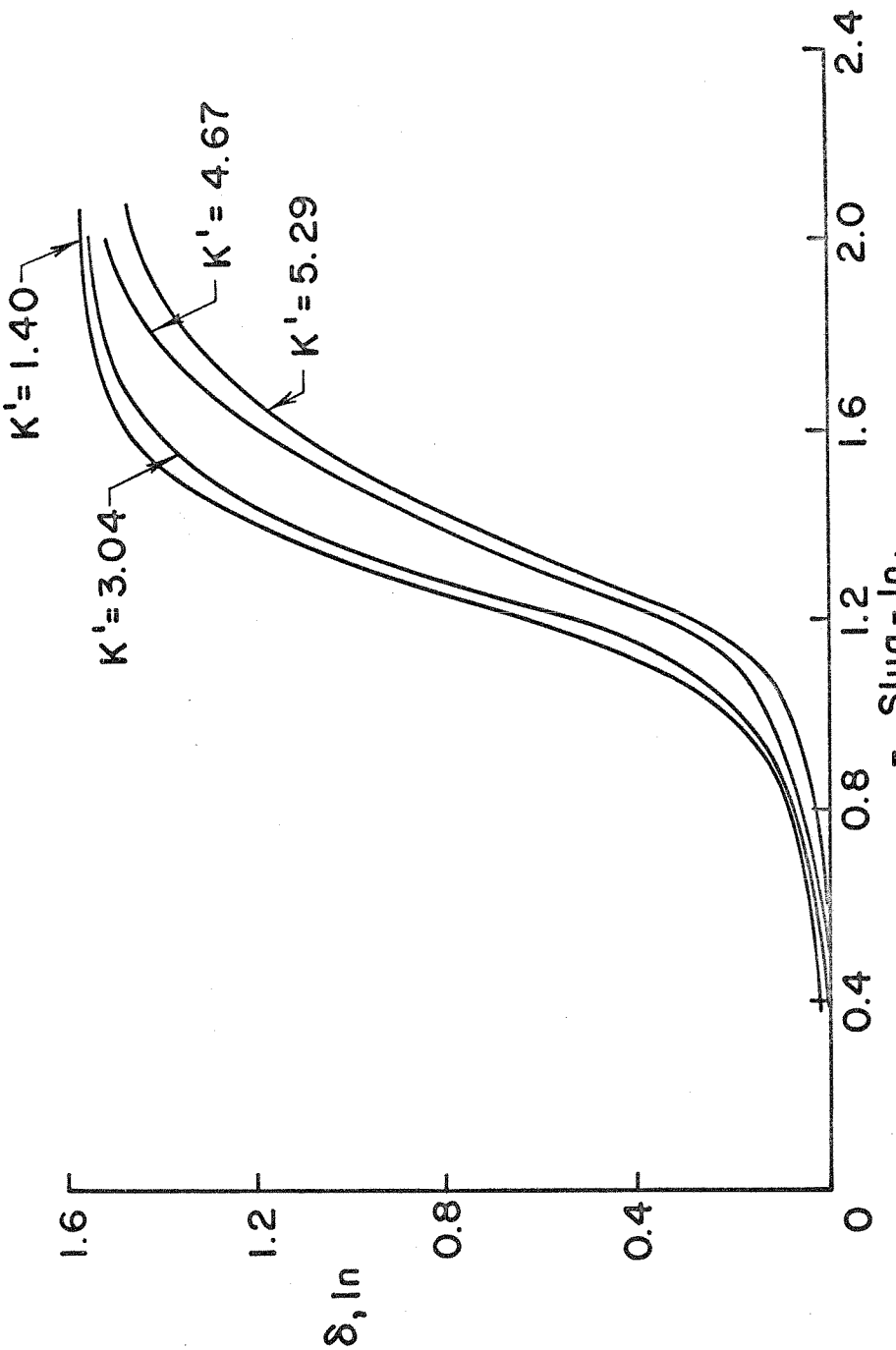

FIG. 10 SUPERIMPOSED ARCH RESPONSES

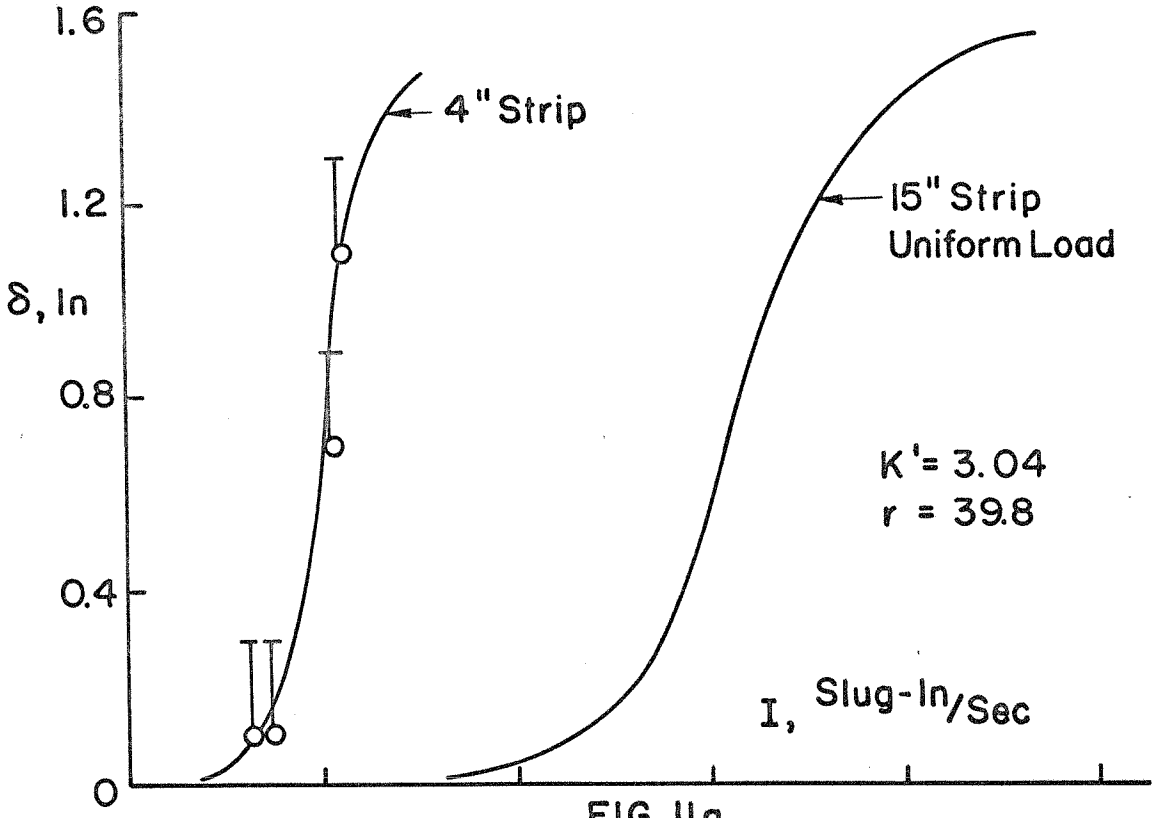

FIG. IIa

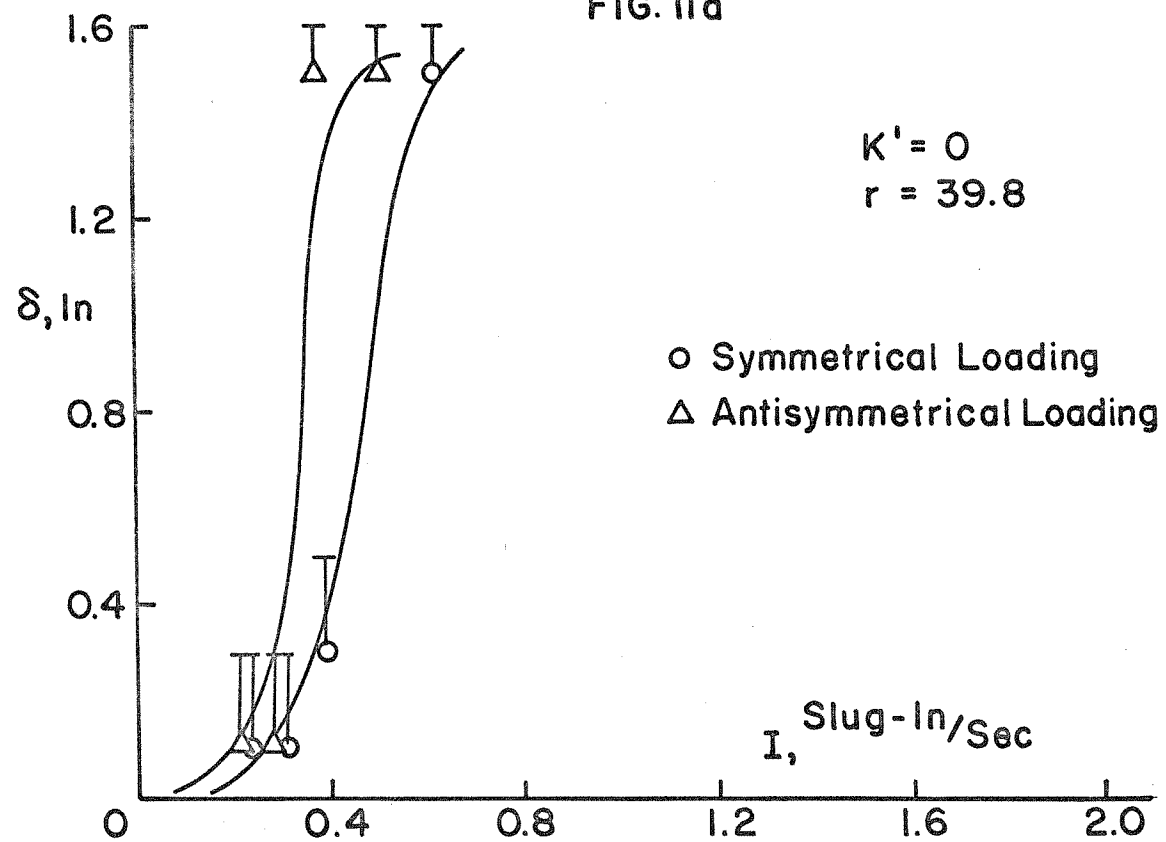

FIG. IIb RESPONSE FOR NON-UNIFORM LOAD

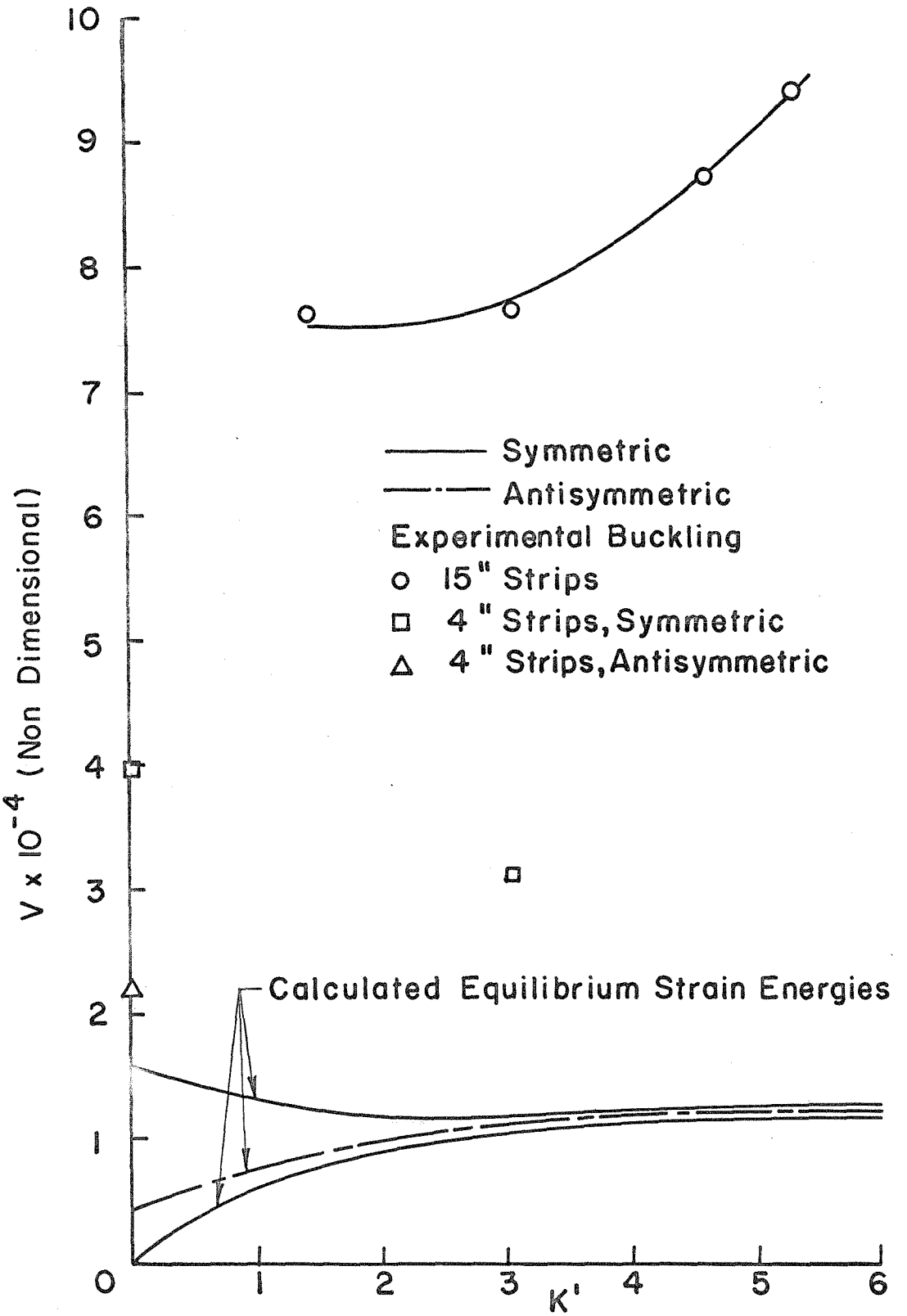

FIG. 12 EXPERIMENTAL BUCKLING POINTS AND EQUILIBRIUM STRAIN ENERGIES